Syst., T. G. Dietterich, S. Becker, and Z. Ghahramani, Eds., 2002, vol. 14, pp. 793–800.
[10] W. Ilg, G. H. Bakir, J. Mezger, and M. A. Giese, "On the representation, learning and transfer of spatio-temporal movement characteristics," *Int. J. Humanoid Robot.*, vol. 1, no. 4, pp. 613–636, 2004.
[11] W. Takano and Y. Nakamura, "Humanoid robot's autonomous acquisition of proto-symbols through motion segmentation," in *Proc. IEEE Int. Conf. Humanoid Robots*, 2006, pp. 425–431.
[12] Y. Kuniyoshi, M. Inaba, and H. Inoue, "Teaching by showing: Generating robot programs by visual observation of human performance," in *Proc. Int. Symp. Ind. Robots*, 1989, pp. 119–126.
[13] Y. Kuniyoshi and H. Inoue, "Learning by watching: Extracting reusable task knowledge from visual observation of human performance," *IEEE Trans. Robot. Autom.*, vol. 10, no. 6, pp. 799–822, Dec. 1994.
[14] S. Liu and H. Asada, "Transferring manipulative skills to robots: Representation and acquisition of tool manipulative skills using a process dynamics model," *J. Dyn. Syst., Meas. Control*, vol. 114, no. 2, pp. 220–228, 1992.
[15] R. Dillmann, O. Rogalla, M. Ehrenmann, R. Zollner, and M. Bordegoni, "Learning robot behaviour and skills based on human demonstration and advice: The machine learning paradigm," in *Proc. Int. Symp. Robot. Res.*, 1999, pp. 229–238.
[16] K. Bernardin, K. Ogawara, K. Ikeuchi, and R. Dillmann, "A sensor fusion approach for recognizing continuous human grasping sequences using hidden Markov models," *IEEE Trans. Robot.*, vol. 21, no. 1, pp. 47–57, Feb. 2005.
[17] A. Billard, S. Calinon, and F. Guenter, "Discriminative and adaptive imitation in uni-manual and bi-manual tasks," *Robot. Auton. Syst.*, vol. 54, pp. 370–384, 2006.
[18] T. Asfour, F. Gyarfas, P. Azad, and R. Dillmann, "Imitation learning of dual-arm manipulation tasks in humanoid robots," in *Proc. IEEE Int. Conf. Humanoid Robots*, 2006, pp. 40–47.
[19] T. Inamura, I. Toshima, H. Tanie, and Y. Nakamura, "Embodied symbol emergence based on mimesis theory," *Int. J. Robot. Res.*, vol. 23, no. 4–5, pp. 363–377, 2004.
[20] A. J. Ijspeert, J. Nakanishi, and S. Schaal, "Movement imitation with nonlinear dynamical systems in humanoid robots," in *Proc. IEEE Int. Conf. Robot. Autom.*, 2002, pp. 1398–1403.
[21] M. Okada, K. Tatani, and Y. Nakamura, "Polynomial design of the nonlinear dynamics for the brain-like information processing of whole body motion," in *Proc. IEEE Int. Conf. Robot. Autom.*, 2002, pp. 1410–1415.
[22] G. W. Taylor, G. E. Hinton, and S. Roweis, "Modeling human motion using binary latent variables," in *Proc. Conf. Neural Inform. Process. Syst.*, 2006, pp. 1345–1352.
[23] S. Calinon, F. Guenter, and A. Billard, "On learning, representing and generalizing a task in a humanoid robot," *IEEE Trans. Syst., Man, Cybern. B, Cybern.*, vol. 37, no. 2, pp. 286–298, Apr. 2007.
[24] O. C. Jenkins and M. Matarić, "Performance-derived behavior vocabularies: Data-driven acquisition of skills from motion," *Int. J. Humanoid Robot.*, vol. 1, no. 2, pp. 237–288, 2004.
[25] D. Kulić, W. Takano, and Y. Nakamura, "Incremental learning, clustering and hierarchy formation of whole body motion patterns using adaptive hidden Markov chains," *Int. J. Robot. Res.*, vol. 27, no. 7, pp. 761–784, 2008.
[26] D. Kulić, D. Lee, Ch. Ott, and Y. Nakamura, "Incremental learning of full body motion primitives for humanoid robots," in *Proc. IEEE Int. Conf. Humanoid Robots*, 2008, pp. 326–332.
[27] B. Janus and Y. Nakamura, "Unsupervised probabilistic segmentation of motion data for mimesis modeling," in *Proc. IEEE Int. Conf. Adv. Robot.*, 2005, pp. 411–417.
[28] L. R. Rabiner, "A tutorial on hidden Markov models and selected applications in speech recognition," *Proc. IEEE*, vol. 77, no. 2, pp. 257–286, Feb. 1989.
[29] B. Janus, "On-line motion segmentation algorithm for mimesis model," Master's thesis, Univ. Tokyo, Tokyo, Japan, 2006.
[30] K. R. Dixon, J. M. Dolan, and P. K. Khosla, "Predictive robot programming: Theoretical and experimental analysis," *Int. J. Robot. Res.*, vol. 23, no. 9, pp. 955–973, 2004.
[31] A. K. Jain, M. N. Murty, and P. J. Flynn, "Data clustering: A review," *ACM Comput. Surveys*, vol. 31, no. 3, pp. 264–323, 1999.
[32] K. Yamane and Y. Nakamura, "Natural motion animation through constraining and deconstraining at will," *IEEE Trans. Vis. Comput. Graph.*, vol. 9, no. 3, pp. 352–360, Jul.–Sep. 2003.
[33] D. Kulić (2009). Supplementary on-line material [Online]. Available: http://www.ynl.t.u-tokyo.ac.jp/∼dana/TRO2009SuppMaterial.html

Source Seeking for Two Nonholonomic Models of Fish Locomotion

Jennie Cochran, Eva Kanso, Scott D. Kelly, Hailong Xiong, and Miroslav Krstic

***Abstract*—In this paper, we present a method of locomotion control for underwater vehicles that are propelled by a periodic deformation of the vehicle body, which is similar to the way a fish moves. We have developed control laws employing "extremum seeking" for two different "fish" models. The first model consists of three rigid body links and relies on a 2-degree-of-freedom (DOF) movement that propels the fish without relying on vortices. The second fish model uses a Joukowski airfoil that has only 1 DOF in its movement and, thus, relies on vortex shedding for propulsion. We achieve model-free and position-free "source seeking," and, if position is available, navigation along a predetermined path.**

***Index Terms*—Adaptive control, localization.**

I. Introduction

The literature on underwater vehicles has started to address vehicles that are propelled forward by periodic shape deformations that are similar to the movement of fish. In this paper, we apply our extremum-/source-seeking method [4], [5] to two different "fish" models and achieve the same results in each case: The fish achieves source localization in underwater environments, and if position measurement is available, it is capable of navigating along a predetermined path.

The fish models are distinguished by their respective underlying methods of propulsion. The first fish model, developed by Kanso *et al.* [8], relies on a 2-degree-of-freedom (DOF) *nonreciprocal* movement, namely, out-of-phase movement at the two joints, which propels the fish through a perfect fluid without the use of a Kutta condition to shed vortices. The second fish model, which has been developed by Xiong [30] (and studied by Mason [14]), has only 1 DOF in its movement and relies on vortex shedding to move through a perfect fluid (by the *scallop theorem* [24], a 1-DOF vehicle cannot locomote in a perfect irrotational fluid). In both models, the fish can propel and turn itself by periodically changing its shape. In this paper, we study how to use a combination of these two "gaits" for source seeking.

Much work has been done in the area of modeling fish movement for control [6], [8], [14], [30]. Kanso *et al.* [8] use conservation of circulation and ideas from reduction theory to build a model for a three-link fish without the explicit use of the fluid variables. This enables [8] to explicitly derive the equations of motion for the fish model and to study the locomotion solely due to body shape changes and not from vorticity.

Manuscript received November 24, 2008; revised June 16, 2009. First published July 24, 2009; current version published October 9, 2009. This paper was recommended for publication by Associate Editor W. Chung and Editor K. Lynch upon evaluation of the reviewers' comments. This work was supported by the National Defense Science and Engineering Graduate Fellowship, by the National Science Foundation, and by the Office of Naval Research under Grant N00014-07-1-0741.

J. Cochran and M. Krstic are with the Department of Mechanical and Aerospace Engineering, University of California, San Diego, CA 92093 USA (e-mail: krstic@ucsd.edu).

E. Kanso is with the Department of Aerospace and Mechanical Engineering, University of Southern California, Los Angeles, CA 90089 USA (e-mail: kanso@usc.edu).

S. D. Kelly is with the Department of Mechanical Engineering and Engineering Science, University of North Carolina at Charlotte, Charlotte, NC 28223 USA (e-mail: scott@kellyfish.net).

H. Xiong is with the Department of Mechanical and Industrial Engineering, University of Illinois at Urbana-Champaign, Urbana, IL 61801 USA (e-mail: aqualonebear@gmail.com).

Digital Object Identifier 10.1109/TRO.2009.2026500

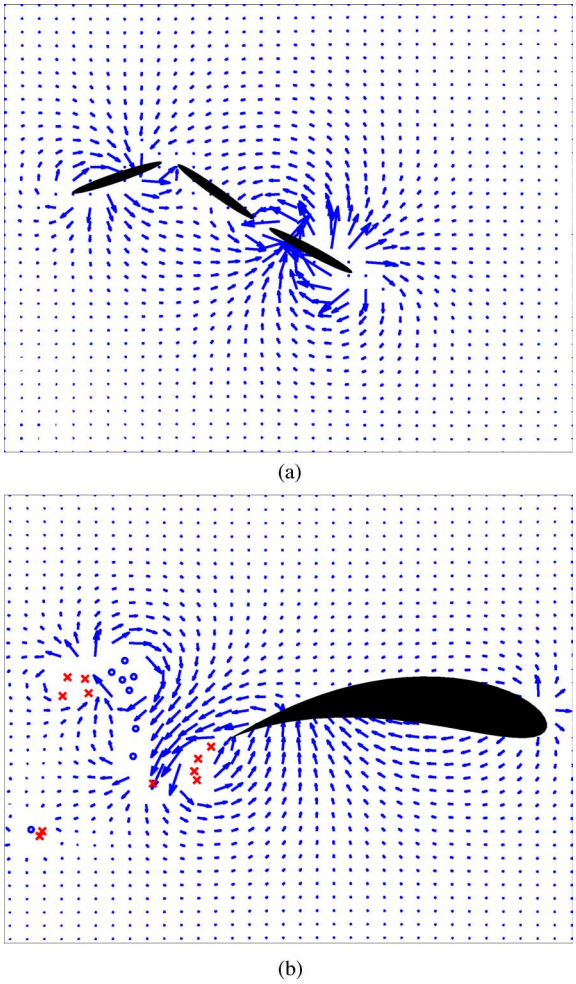

Fig. 1. (a) Three-link fish moving in a potential flow. (b) Joukowski foil fish moving in a flow with point vortices. The arrows represent the velocity vectors of the fluid. The "×"s are point vortices that rotate counter clockwise, while the "○"s are point vortices that rotate clockwise.

The model developed in [14] and [30] spans the gap between the studies that look at deformable bodies moving through a fluid without the use of vortex shedding and studies of systems with rigid bodies and vortices. The Joukowski airfoil fish model relies on only one input and exploits the presence of vortices for both propulsion and steering. Many research groups [9], [14], [15], [17] have developed underwater vehicles that use biology-inspired periodic motion for propulsion. Related work [23] studies stabilization of vortex shedding.

A common theme in all these works is the periodic movement of the body. This brings the extremum-seeking method [1], [12] to mind, as it takes the advantage of periodic probing signals for gradient estimation. We combine the natural gait of the fish model with the extremum seeking for nonmodel-based optimization.

We review our study on source seeking for a nonholonomic unicycle in Section II. Section III discusses the motion of the fish and fluid systems. Section IV specifically discusses a three-link body moving in a fluid, while Section V describes a deformable Joukowski foil moving in a fluid with discrete vortex shedding. In each of the two sections, we present the results of applying extremum-seeking control.

Fig. 1(a) and (b) gives a preview of the problems that we consider and displays the two fish models, which are shown within fluid velocity fields. For our main result, see Figs. 7 (for the three-link fish) and 12 (for the Joukowski fish).

A clarification is due regarding the use of the terms *extremum seeking* and *source seeking*. Extremum seeking [1], [12], [29] is broad set of methods for model-free optimization (for addressing similar problems as genetic programming or simulated annealing but equipped with stability proofs). Source seeking [4], [31], [32] is an application of extremum seeking to real-time *navigation* of dynamics- or kinematics-dominated vehicles to localize extrema in spatially distributed fields, without position measurement and distribution information.

A note is in order on the two models that we consider in this paper and on the notation that we employ. These models are quite nonstandard as control theoretic models, as they consist of ordinary differential equations (ODEs) (the fish subsystem, with forces acting on it included, plus vortex locations and strengths in the case of Joukowski foil fish) and an infinite-dimensional output map (the fluid potential field that allows us to get the entire flow distribution, which is infinite-dimensional, from the finite-dimensional fish state). The three-link fish has five states and two inputs, whereas the Joukowski foil fish has a large number of states (growing to infinity in a "countable" manner as time goes to infinity) and one input. We develop our notation in this paper so that the two models, which are given in the spirit of geometric mechanics in the original literature [8], [14], [30], are presented here as control-oriented (input–state–output) models.

II. Source Seeking for Unicycle

We solved the problem of seeking the source of a scalar signal for a nonholonomic unicycle with constant forward velocity and no position information in [4]. The signal distribution in space is not known, except that it decays with distance from the source.

While other groups have considered source-seeking problems (see [19] and [22]), this paper is different in that the vehicle has no knowledge of its position or the position of the source, there is no communication between it and other entities, and it has nonholonomic dynamics. Many groups have employed unicycle models in their work, including [7] and [11], while others have used the extremum-seeking method in their studies outside of the field of autonomous vehicles, including [2], [3], [10], [13], [20], [21], [27], [28], and [33].

The center r_c of the unicycle is governed by $\dot{r}_c = V_c e^{i\theta}$, where θ is its orientation, and V_c is its constant forward velocity. The sensor position is $r_s = r_c + Re^{i\theta}$. The control is applied through angular velocity as $\dot{\theta} = a\omega\cos(\omega t) + c\xi\sin(\omega t)$, with $\xi = s/(s+h)J$, where $J(r_s(t))$ is the signal sensed at the location of the vehicle sensor $r_s(t)$, which is at a distance R away from the center, and $a, \omega, c,$ and h are the parameters that affect the performance. The control law is made of two terms that serve two different functions. The first term $a\omega\cos(\omega t)$ is a persistent excitation that allows the vehicle to probe the signal space. The second term $c\xi\sin(\omega t)$ is a tuning term that steers the vehicle toward the source based on the estimate of the (average) gradient. In [4], we prove the convergence to a small set near the source using averaging.

III. Equations of Motion in a Perfect Fluid

Two fish models are considered: the articulated body model discussed in [8] and the Joukowski airfoil model discussed in [30]. In both models, the fluid is considered to be inviscid (no viscosity) and incompressible. The presence of viscosity would affect the timing aspects of the locomotion process and attenuate the amplitudes of periodic signals. The tree-link fish would be slowed in its forward motion, and steering ability of extremum seeking would be reduced due to the phase lag. For the Joukowski fish, the vortices would be attenuated, which,

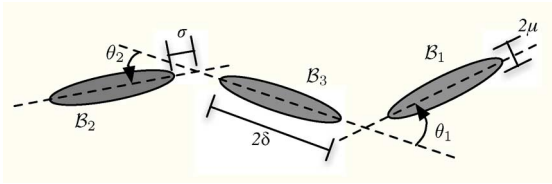

Fig. 2. Configuration of the three-link fish model.

combined with skin friction, would lead to less-efficient propulsion and steering.

The model in [8] does not account for *a vortex shedding mechanism*, and the configuration space of the body fluid system can be identified only with that of the submerged body. Vorticity is shed from the trailing edge of the airfoil in the form of point vortices in [30]. Away from the shed point vortices, the fluid is assumed to remain irrotational at all time. In this case, the configuration space of the body fluid system can be identified with that of the submerged body and the position of the shed point vortices.

The fluid velocity field $\mathbf{u}$, which is in the fluid domain, excluding the body and point vortices when accounted for, can be expressed in terms of a potential function ϕ as $\mathbf{u} = \nabla\phi$. Incompressibility implies that $\nabla^2\phi = 0$. The boundary conditions result from the two assumptions that the fluid is at rest at infinity and that fluid particles may slip along the body surface and are expressed as $\mathbf{u}|_\infty = 0$ and $\mathbf{u}\cdot\mathbf{n} = \dot{\mathcal{B}}|_{\mathcal{S}}\cdot\mathbf{n}$, where $\mathcal{B}$ is the set of points representing the fish body, and $\mathcal{S}$ is the surface of the body (touching the fluid). In the articulated body model [8], the potential function ϕ is a function of the configuration and velocity of the body and is computed numerically using a boundary element method [26]. In the case of the Joukowski airfoil [14], [30], ϕ is a function of the configuration and velocity of the body, as well as the position of the shed point vortices, and is obtained in a closed form using tools from complex analysis.

The kinetic energy of the fluid is $T_f = (1/2)\int_{\mathcal{D}}\mathbf{u}^2 dv$, where $\mathcal{D}$ is the fluid domain (excluding singularities present in the form of point vortices), and dv is the standard volume element. Using Green's theorem, $T_f = -(1/2)\int_{\partial S}\phi\nabla\phi\cdot\mathbf{n}ds$, where ∂S is the surface of the fish body, and $\mathbf{n}$ is the unit normal into the fluid. Expressions of T_f for each model in terms of the body variables and the body variables plus position of point vortices are presented in Sections IV and V.

The equations governing the net locomotion of the fish in both models are variations of Kirchhoff's equations for the motion of a rigid body in an ideal fluid (see [16])

$$\frac{d\mathbf{L}}{dt} + \Omega\mathbf{k}\times\mathbf{L} = 0, \qquad \frac{dA}{dt} + \mathbf{k}([U\ V]^T\times\mathbf{L}) = 0 \tag{1}$$

where $\mathbf{L}$ and A are the linear and angular momenta of the body fluid system, and U, V, and Ω are the translational and rotational velocities associated with a net locomotion of the body. The variables $\mathbf{L}$, A, U, V, and Ω are expressed in a body frame moving with the fish. The linear and angular momenta $\mathbf{L}$ and A are obtained by differentiating the kinetic energy of the system $\mathbf{L} = [\partial T/\partial U,\ \partial T/\partial V]^T$, $A = \partial T/\partial\Omega$. With conservation of momentum and starting the system from rest, which, in turn, implies $\mathbf{L} = 0$ and $A = 0$ for all time, one solves for U, V, and Ω at each time step and then integrates them to derive the locomotion of the fish.

IV. Source Seeking for a Three-Link Fish

Consider the articulated fish model discussed in [8] and formed by three identical rigid links connected via hinge joints that allow the links to rotate relative to each other. As depicted in Fig. 2, each link $\mathcal{B}_i$ of the fish is an ellipse with semimajor axis of length δ and semiminor axis of length μ. The joints that connect the links are located at a distance σ away from the tips of the ellipses, and the relative angles are denoted by θ_α, where $\alpha = 1$ and 2. The two inputs to the system are the angular velocities of the two joints $\dot\theta_1$ and $\dot\theta_2$.

A. ODE Model With a Function-Valued Output Map for a Three-Link Fish in a Potential Flow

As shown in [8], five state variables completely describe the shape, as well as the position and orientation, of the three-link fish relative to an inertial frame. These five variables are given by the vector $\Xi = [\theta_1\ \theta_2\ g_3^T]^T$, where $g_3 = [\theta_f\ f_x\ f_y]^T$, and (f_x, f_y) and θ_f are, respectively, the location of the center of the middle ellipse and the orientation of the middle ellipse with respect to the fixed inertial frame. The inputs to the system are the angular velocities of the joints, where $\Psi = [\Psi_1\ \Psi_2]^T$, i.e., $\dot\theta_1 = \Psi_1$ and $\dot\theta_2 = \Psi_2$, while the function-valued output map is the potential field $\phi(x,y) = \eta[\Xi,\Psi](x,y)$, which is governed by the Laplace equation $\nabla^2\phi = 0$ and the solution operator $\eta[\Xi,\Psi]$, which is defined shortly.

To complete this description, we explain the governing ODE for $\dot g_3$. Each link $\mathcal{B}_i$ is defined by an orientation and position $g_i = [\theta_{\mathcal{B}_i}\ \mathcal{B}_{ix}\ \mathcal{B}_{iy}]^T$ with respect to a fixed inertial frame. The angular and translational velocities are expressed with respect to the fixed inertial frame as $\dot g_i$ or, with respect to their own body frame, as $\xi_i = [\Omega_i, U_i, V_i]^T$, where $i = 1, 2,$ and 3. The relationship between $\dot g_3$ and ξ_3 is defined by

$$\dot g_3 = \Upsilon\xi_3 \qquad \Upsilon(\theta_f) = \begin{bmatrix} 1 & 0 & 0 \\ 0 & \cos(\theta_f) & -\sin(\theta_f) \\ 0 & \sin(\theta_f) & \cos(\theta_f) \end{bmatrix} \tag{2}$$

where we must still explain the relationship between ξ_3 and (Ξ,Ψ). The entire configuration is defined through the movement of one link (the middle link $\mathcal{B}_3$ is the link of choice) plus the movement of the joints, i.e., the entire system can be defined by the state variables Ξ. With this in mind, the velocities of the other two links relative to the third link, but expressed with respect to their respective fixed frames, are $\zeta_1 = \xi_1 - \mathrm{Ad}_{x_1^{-1}}\xi_3$ and $\zeta_2 = \xi_2 - \mathrm{Ad}_{x_2^{-1}}\xi_3$, where $\mathrm{Ad}_{x_1^{-1}}(\theta_1)$ and $\mathrm{Ad}_{x_2^{-1}}(\theta_2)$ are defined as

$$\mathrm{Ad}_{x_1^{-1}} = \begin{bmatrix} 1 & 0 & 0 \\ (\delta+\sigma)\sin(\theta_1) & \cos(\theta_1) & \sin(\theta_1) \\ (\delta+\sigma)(1+\cos(\theta_1)) & -\sin(\theta_1) & \cos(\theta_1) \end{bmatrix}$$

$$\mathrm{Ad}_{x_2^{-1}} = \begin{bmatrix} 1 & 0 & 0 \\ -(\delta+\sigma)\sin(\theta_2) & \cos(\theta_2) & \sin(\theta_2) \\ -(\delta+\sigma)(1+\cos(\theta_2)) & -\sin(\theta_2) & \cos(\theta_2) \end{bmatrix}$$

and transform ξ_3 from the $\mathcal{B}_3$-fixed frame to the $\mathcal{B}_1$-fixed and $\mathcal{B}_2$-fixed frames. The variables ζ_1 and ζ_2 are given by $\zeta_1 = \Pi_1\dot\theta_1 = \Pi_1\Psi_1$ and $\zeta_2 = \Pi_2\dot\theta_2 = \Pi_2\Psi_2$, where $\Pi_1 = [1\ \ 0\ \ +(\delta+\sigma)]^T$, and $\Pi_2 = [1\ \ 0\ \ -(\delta+\sigma)]^T$.

The kinetic energy of the fluid T_f, where $\partial S = \sum_1^3\partial\mathcal{B}_i$ is the boundary over all three bodies, can be expressed in terms of "added inertias" $\mathbb{M}_{ij}^f$ and ξ_i as $T_f = (1/2)\sum_{i=1}^3\sum_{j=1}^3\xi_i^T\mathbb{M}_{ij}^f(\Xi)\xi_j$. The "added inertias" $\mathbb{M}_{ij}^f$ depend on the configuration of the three-link body Ξ and are derived in [8]. This is a consequence of being able to express ϕ solely in terms of the body configuration and velocities $\phi = \sum_{i=1}^3(\Omega_i\mathcal{X}_i + [U_i, V_i]\varphi_i) = \sum_{i=1}^3[\mathcal{X}_i\ \varphi_i^T]\xi_i$, where $\mathcal{X}_i(x,y,\Xi)$ and $\varphi_i(x,y,\Xi)$ define potential functions that depend

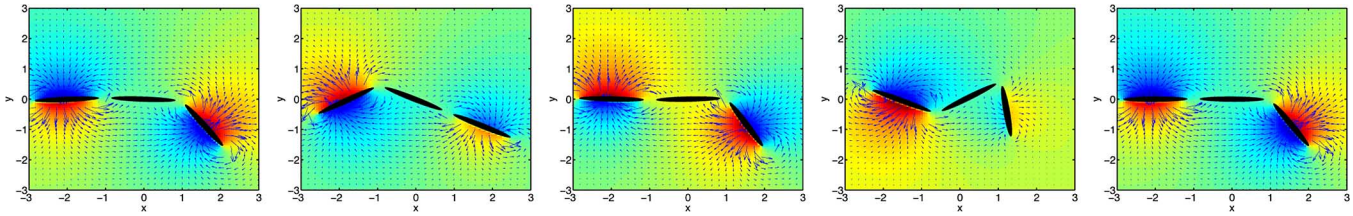

Fig. 3. Snapshots in time of reciprocal motion. The background color field represents the potential field ϕ with red representing positive values and blue representing negative values. $\beta_0 = 1$, and $\theta_1|_{t=0} = -1$, $\theta_2|_{t=0} = 0$.

only on θ_1, θ_2, and g_3 and on the spatial coordinates (x, y). The quantities $\mathcal{X}_i$ and φ_i depend on coefficients that are found using a boundary element method [26] and depend only on Ξ and not on the spatial coordinates. These coefficients are used to find $\mathbb{M}^f_{ij}(\Xi)$. The kinetic energy of the bodies $T_{\mathcal{B}_i} = (1/2)(\mathcal{I}\Omega_i^2 + m(U_i^2 + V_i^2))$ can also be expressed in terms of ξ_i as $T_{\mathcal{B}_i} = (1/2)\xi_i^T \mathbb{M}^b_i \xi_i$, where $\mathbb{M}^b_i = \text{diag}\{\mathcal{I}, m, m\}$, where m is the mass of the ellipse, and $\mathcal{I} = m(a^2 + b^2)/4$ is the body moment of inertia. The total kinetic energy of the system is then expressed as $T = (1/2)\sum_{i=1}^3 \sum_{j=1}^3 \xi_i^T \mathbb{I}_{ij} \xi_j$, $\mathbb{I}_{ij} = \mathbb{M}^f_{ij}(\Xi)$, for $i \neq j$, and $\mathbb{I}_{ii} = \mathbb{M}^f_{ii}(\Xi) + \mathbb{M}^b_i$. The total effective momentum $h_s = [A\ \mathbf{L}^T]^T$ expressed with respect to the $\mathcal{B}_3$ fixed frame is $h_s = \sum_{i=1}^3 \sum_{j=1}^3 \text{Ad}^T_{x_i^{-1}} \mathbb{I}_{ij} \xi_j$, where $\text{Ad}^T_{x_i^{-1}}(\theta_i)$ transforms from the $\mathcal{B}_i$-fixed frame to the $\mathcal{B}_3$-fixed frame. (Note that $\text{Ad}^T_{x_3^{-1}}$ is the identity operator.) Equation for h_s can now be rewritten as $h_s = \sum_{i=1}^3 \text{Ad}^T_{x_i^{-1}} \mathbb{I}_{i3} \xi_3 + \sum_{i=1}^3 \sum_{\alpha=1}^2 \text{Ad}^T_{x_i^{-1}} \mathbb{I}_{i\alpha} (\zeta_\alpha + \text{Ad}_{x_\alpha^{-1}} \xi_3)$ and is governed by Kirchhoff-like equations. As we assume that the system starts from rest, h_s remains zero for all time. This leads to $\xi_3(\Xi, \Psi) = -(\sum_{i=1}^3 \text{Ad}^T_{x_i^{-1}} \mathbb{I}_{i3} + \sum_{i=1}^3 \sum_{\alpha=1}^2 \text{Ad}^T_{x_i^{-1}} \mathbb{I}_{i\alpha} \text{Ad}_{x_\alpha^{-1}})^{-1} \sum_{i=1}^3 \sum_{\alpha=1}^2 \text{Ad}^T_{x_i^{-1}} \mathbb{I}_{i\alpha} \Pi_\alpha \Psi_\alpha$.

Thus, the input–state–output model of the system is

$$\dot{\Xi} = [\ \Psi_1,\ \Psi_2,\ l(\Xi, \Psi)^T\ ]^T \tag{3}$$

$$\eta[\Xi, \Psi](x, y) = \tau_1(\Xi, \Psi)^T \Pi_1 \Psi_1 + \tau_2(\Xi, \Psi)^T \Pi_2 \Psi_2 + \sum_{i=1}^3 \tau_i(\Xi, \Psi)^T \Gamma_i(\Xi) \xi_3(\Xi, \Psi) \tag{4}$$

where $l = [l_1\ l_2\ l_3]^T = \Upsilon(\theta_f)\xi_3, \tau_i(\Xi, \Psi) = [\mathcal{X}_i(x, y, \Xi)\ \varphi_i^T(x, y, \Xi)]^T, \Gamma_1 = \text{Ad}_{x_1^{-1}}(\theta_1), \Gamma_2 = \text{Ad}_{x_2^{-1}}(\theta_2)$, and $\Gamma_3 = I$. Therefore, the complete dynamic system is given by the 5-D state equation (3) and the function-valued output map (4).

B. Basic Gaits for Three-Link Fish

Reciprocal (in-phase) motion, such as $\dot{\theta}_1 = \cos(t), \dot{\theta}_2 = \beta_0 \cos(t)$, and $\beta_0 \in \Re$, results in no net forward movement, as shown in Fig. 3. We consider two basic *nonreciprocal* gaits: moving forward and turning [8]. The angular velocities for both gaits are the same as

$$\dot{\theta}_1 = a\omega \sin(\omega t), \qquad \dot{\theta}_2 = a\omega \cos(\omega t) \tag{5}$$

but the initial condition differs. The initial conditions to move forward are $\theta_1|_{t=0} = -a, \theta_2|_{t=0} = 0$, leading to $\theta_1 = -a\cos(\omega t), \theta_2 = \sin(\omega t)$. However, the initial conditions for turning are $\theta_1|_{t=0} = \beta - a$ and $\theta_2|_{t=0} = -\beta$, leading to

$$\theta_1 = -a\cos(\omega t) + \beta, \qquad \theta_2 = a\sin(\omega t) - \beta\,. \tag{6}$$

Note that $\beta = a = \omega = 1$ in [8]. Fig. 4 shows the fish moving forward for different parameter combinations, while Fig. 5 shows the fish turning in circles for different parameter combinations. Fig. 6 shows snapshots in time of the fish moving forward.

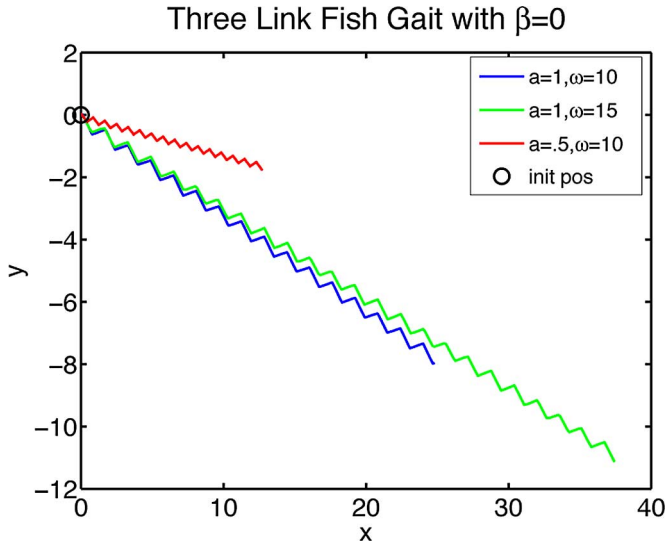

Fig. 4. Forward gaits of a three-link fish. $\beta = 0$.

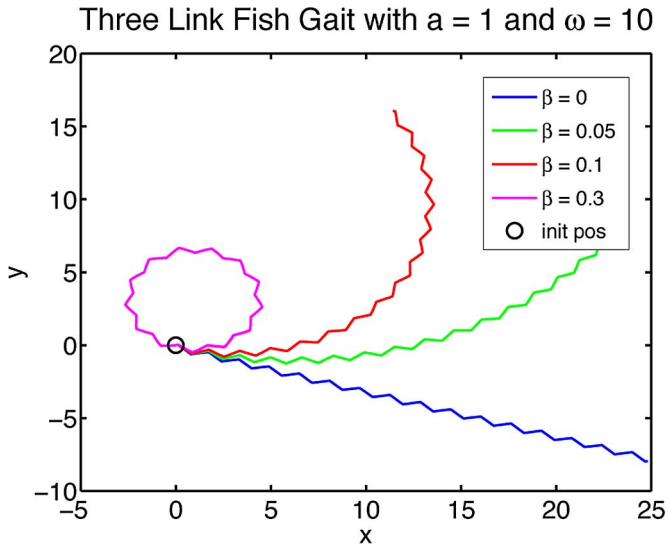

Fig. 5. Turning gaits of a three-link fish. $a = 1$, and $\omega = 10$.

C. Source Seeking With a Three-Link Fish

We take the basic gaits of the three-link fish and modify them. There are two parts to our control law: 1) how to apply extremum seeking to the gaits and 2) what function to optimize with extremum seeking.

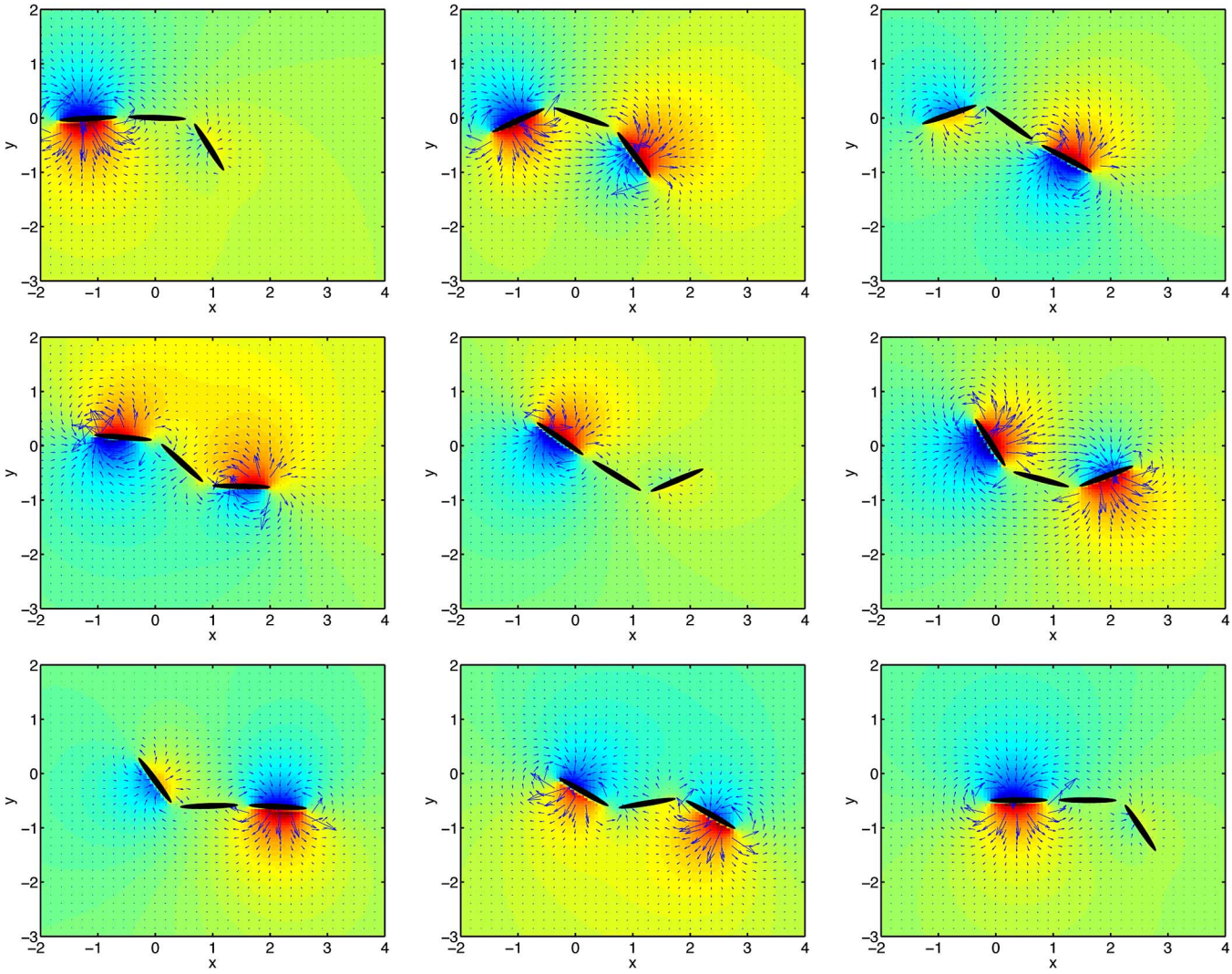

Fig. 6. Snapshots in time of the fish moving forward. The background color field represents the potential field ϕ with red representing positive values and blue representing negative values. $a = 1$, $\theta_1|_{t=0} = -1$, and $\theta_2|_{t=0} = 0$.

As explained in Section II, the control law for the nonholonomic unicycle is made up of two parts: the probing term $a\omega\cos(\omega t)$ and the tuning/steering term $c\xi\sin(\omega t)$. The probing $a\omega\cos(\omega t)$ is exactly what we see in (5), modulo a phase shift. If we assume that β depends on time instead of being constant, and then, by following (6), we find $\dot{\theta}_1 = a\omega\sin(\omega t) + \dot{\beta}$ and $\dot{\theta}_2 = a\omega\cos(\omega t) - \dot{\beta}$. By equating $\dot{\beta} = -c\xi\cos(\omega t)$, we arrive at our control law

$$\dot{\theta}_1 = a\omega\sin(\omega t) - c\xi\cos(\omega t) \tag{7}$$

$$\dot{\theta}_2 = a\omega\cos(\omega t) + c\xi\cos(\omega t) \tag{8}$$

$$\xi = \frac{s}{s+h}[J] \tag{9}$$

where J is the signal that we want to maximize. (The transfer function $s/(s+h)$ should be understood as an operator on functions of time, rather than as mixing of time and frequency domain quantities.) If the source location is (x^*, y^*), the signal that the fish senses is

$$J = -q_r((f_{sx} - x^*)^2 + (f_{sy} - y^*)^2) \tag{10}$$

$$f_s = \begin{bmatrix} f_x + \cos(\theta_f)(\delta+\sigma) + \cos(\theta_1+\theta_f)(2\delta+\sigma) \\ f_y + \sin(\theta_f)(\delta+\sigma) + \sin(\theta_1+\theta_f)(2\delta+\sigma) \end{bmatrix} \tag{11}$$

where $q_r > 0$, and $f_s = (f_{sx}, f_{sy})$ is the location of the sensor that we assume to be at the tip of the forward ellipse, i.e., the fish nose. Fig. 7 shows a typical simulation of the fish moving to a desired location under the algorithms (7)–(9). This simulation was made while enforcing the constraint that the tuning variable β does not exceed a certain value—the amplitude of the probing signal a. This ensures that the links do not cross themselves as the fish moves. With measurement of $J(t)$, the fish reaches J^* without position measurement.

D. Path Following for a Three-Link Fish

The function J can be modified so that the fish follows a predefined path. We define the target path $x = a_1y^3 + a_2y^2 + a_3y + a_4$ and define J as a function of the error between f_{sx} and $a_1f_{sy}^3 + a_2f_{sy}^2 + a_3f_{sy} + a_4$. The error can be multiplied by a gain, and can be raised to a power to obtain different gradient fields. Fig. 8 shows the fish following the path defined by $x = 2/300y^3 - 2/5y^2 + 16/3y + 1$. The fish optimizes

$$J = -5\sqrt{\left|f_{sx} - \frac{2}{300}f_{sy}^3 - \frac{2}{5}f_{sy}^2 + \frac{16}{3}f_{sy} + 1\right|} \tag{12}$$

to follow this path.

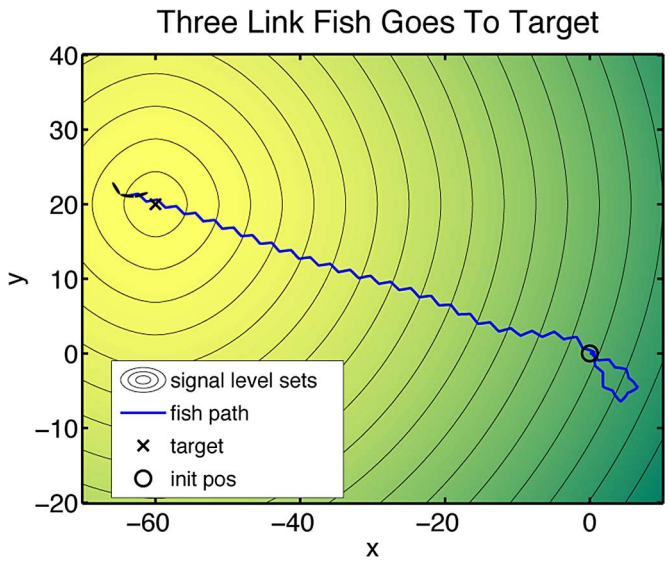

Fig. 7. Source seeking for a three-link fish. The background color field represents the "concentration" of the signal field J with yellow representing higher values than green. $a = 1$, $c = 2$, $\omega = 10$, $h = 10$, $q_r = 1/100$, $\delta = 5/6$, and $\sigma = 1/6$.

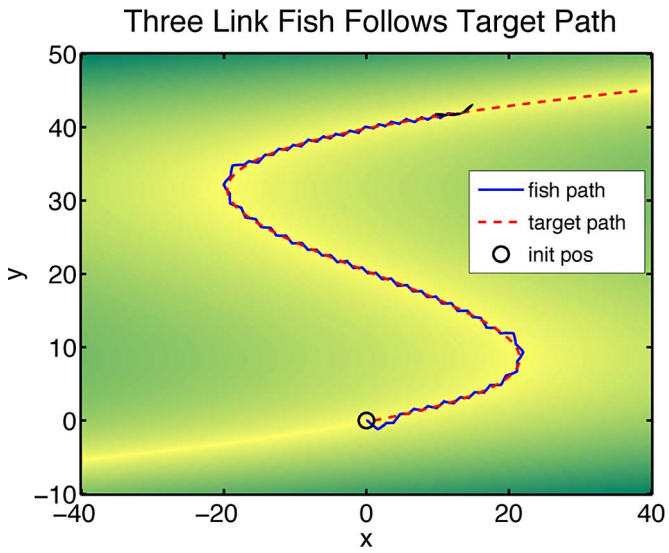

Fig. 8. Three-link fish following a predetermined path. The background color field represents the "concentration" of the signal field J with yellow representing higher values than green. $a = 1$, $c = 2$, $\omega = 10$, $h = 10$, $\delta = 5/6$, and $\sigma = 1/6$.

V. Source Seeking for a Joukowski Foil Fish

We now move to the discussion of locomotion for a deformable Joukowski foil [14], [30]. The transformation $z = F(\zeta) = \zeta + \zeta_c + \alpha/(\zeta + \zeta_c)$ allows the parameterization of a circle $\zeta = r_c e^{i\theta}$ in the ζ-plane to describe an airfoil in the $z = x + iy$ plane. The parameters $\zeta_c = \zeta_x + i\zeta_y \in \mathbb{C}$ and $\alpha \in \mathbb{R}$ determine the foil shape. Varying the imaginary part $\Im\{\zeta_c\} = \zeta_y$, while enforcing the constraint $r_c = |\zeta_c - \alpha|$ with r_c constant, causes the camber of the foil to vary as well. This variation allows for 1 DOF, which, by itself, will not allow the fish to make forward progress in a potential flow. To counter this, [14] and [30] add discrete point vortices to the system, which are modeled after vortex shedding by the actual fish. (The potential function in this case encompasses the domain of the fluid minus small circles at the locations of the vortices.) The vortices are shed at discrete time instants from the trailing edge of the fish. When this happens, an exchange of momentum ensues, and the fish is capable of moving forward. By periodically varying $\dot{\zeta}_y$—the single input to the system—in a certain way, the fish will move forward or turn.

A. ODE Model With Function-Valued Output Map for a Joukowski Foil Fish in a Potential Flow With Point Vortices

The continually growing number of state variables of this system are $\Xi = \left[\zeta_y \;\; g \;\; \Lambda^T \;\; \Gamma^T\right]^T$, where $g = [\theta_f \;\; f_x \;\; f_y]^T$, $\Lambda = [\zeta_1 \;\; \zeta_2 \;\; \ldots]^T$, with $\zeta_k \in \mathbb{C}^N$, is a vector of the location of each point vortex, and $\Gamma = [\gamma_1 \;\; \gamma_2 \;\; \ldots]^T$, with $\gamma_k \in \mathbb{R}$, is a vector of the strength of each point vortex. The variables θ_f and (f_x, f_y) are the orientation and location of the foil fish with respect to the spatially fixed frame. The number of vortices N grows with time; at periodic discrete times, another vortex is added. The system has one input $\dot{\zeta}_y = \Psi$, while the output map defines the potential field and is given in the function-valued form $\phi(x, y) = \eta[\Xi, \Psi](x, y)$.

Both [14] and [30] develop the equations of motion for a Joukowski foil in a perfect fluid with point vortices. Reference [14] develops the expression for the potential function, which is used in [30] (and, therefore, we use as well). However, [14] uses Newton's second law to derive the motion of the body, while [30] applies conservation laws.

The complex potential $W(z) = \phi(z) + i\psi(z)$ is an analytic function, where ϕ is the potential function, and ψ is the stream function. Similar to the three-link fish case, we use a frame of reference attached to the foil and express $W(z)$ in terms of the body configuration and velocities as $w(\zeta) = W(z) = Uw_1(\zeta) + Vw_2(\zeta) + \Omega w_3(\zeta) + \dot{\zeta}_x w_{s1}(\zeta) + \dot{\zeta}_y w_{s2}(\zeta) + \dot{\alpha} w_{s3}(\zeta) + \sum_{k=1}^{N} w_{pv}^k(\zeta)$, where U and V are the translational velocities of the foil, Ω is the rotational velocity, N is the number of vortices in the flow, and $w_{pv}^k(\zeta)$ represents the contribution to the potential from the kth vortex. As noted in [30], the subscript "s" appears in conjunction with variables describing the shape of the foil. Finding the functions w_i and w_{si} corresponds to satisfying the boundary condition that the normal component of the fluid velocity must match the normal component of the velocity of the foil at its surface. The velocity of the foil at its surface is a combination of the translational and rotational velocities of the foil *plus* the velocities associated with the change in shape $\dot{\zeta}_x, \dot{\zeta}_y$, and $\dot{\alpha}$, which depends on the input $\Psi = \dot{\zeta}_y$. The expressions for these functions are listed in the Appendix. The functions w_{pv}^k are found using the *Milne–Thomson circle theorem* [16] as $w_{pv}^k = i\gamma_k(\log(\zeta - \zeta_k) - \log(\zeta - (r_c^2/\zeta_k)))$, where ζ_k is the location of the kth point vortex, and γ_k is its strength.

Using the complex potential $W(z)$, the kinetic energy of the fluid can be determined from the same integral used in Section IV-A as $T_f = -(1/2)\int_{\partial S} \phi(\nabla\phi \cdot \mathbf{n})ds$, where ∂S is the surface of the foil. Given that ϕ is a function of the body configuration, the body velocities, and the point vortices, T_f can be expressed as $T_f = (1/2)[\mathbf{U}^T \;\; \dot{\mathbf{s}}^T \;\; \Gamma^T]\mathbb{M}^{T_f}[\mathbf{U}^T \;\; \dot{\mathbf{s}}^T \;\; \Gamma^T]^T$, $\mathbf{U} = [\Omega \; U \; V]^T$, $\mathbf{s} = [\zeta_x \;\; \zeta_y \;\; \alpha]^T$, and $\Gamma = [\gamma_1 \;\; \ldots \;\; \gamma_N]^T$, where the body shape $\mathbf{s}(\zeta_y)$ can be determined from ζ_y alone, the matrix $\mathbb{M}^{T_f}(\mathbf{s}, \Lambda)$ depends only on the foil *shape* $\mathbf{s}(\zeta_y)$, and the location of the vortices and the change in the body shape $\dot{\mathbf{s}}(\mathbf{s}, \Psi)$ depend only on the shape $\mathbf{s}(\zeta_y)$ and the input Ψ. From the relationship between ζ_y and ζ_x, a is defined as $\zeta_x(\zeta_y) = ((1-\mu)/(1+\mu))\sqrt{r_c^2 - \zeta_y^2}$, and $\alpha(\zeta_y) = \zeta_x - \sqrt{r_c^2 - \zeta_y^2} = -(2\mu/(1+\mu))\sqrt{r_c^2 - \zeta_y^2}$, where $\mu \in (0, 1)$ is a constant. The kinetic energy of the foil can also be expressed in term of the body configuration and velocities $T_{\mathcal{B}} = (1/2)[\mathbf{U}^T \;\; \dot{\mathbf{s}}^T]\mathbb{M}^{T_{\mathcal{B}}}[\mathbf{U}^T \;\; \dot{\mathbf{s}}^T]^T$, where the matrix $\mathbb{M}^{T_{\mathcal{B}}}(\mathbf{s})$ depends on

only the shape $\mathbf{s}$ of the foil. The total effective momentum of the system is $A = ((\partial(T_{\mathcal{B}} + T_f))/\partial\Omega) - (1/2)\sum_{k=1}^{N}(-2\pi\gamma_k)(|\mathbf{z}_k|^2 - |\mathbf{z}_0|^2)$ and $\mathbf{L} = [(\partial(T_{\mathcal{B}} + T_f)/\partial U), (\partial(T_{\mathcal{B}} + T_f)/\partial V)] + \sum_{k=1}^{N}(-2\pi\gamma_k)(\mathbf{z}_k + \mathbf{z}_0)\mathbf{k}$, where the terms due to the vortices are developed in [25], $\mathbf{z}_k = [\Re\{z_k\}\ \Im\{z_k\}]^T$ is the vector location of the kth vortex in the foil-fixed frame, and $\mathbf{z}_0$ is the location of the origin of the foil-fixed frame with respect to the spatially fixed frame. The momentum is governed by (1), and the system starts from rest; therefore, $\mathbf{L} = [L_x\ L_y]^T = 0$ and $A = 0$ for all time. Thus, we have a system of equations

$$\begin{bmatrix} A \\ L_x \\ L_y \end{bmatrix} = I \begin{bmatrix} \Omega \\ U \\ V \end{bmatrix} + B \begin{bmatrix} \dot{\zeta}_x \\ \dot{\zeta}_y \\ \dot{\alpha} \end{bmatrix} + P \begin{bmatrix} \gamma_1 \\ \vdots \\ \gamma_N \end{bmatrix} \tag{13}$$

with a solution $\mathbf{U}(\Xi, \Psi) = -I^{-1}(B\dot{\mathbf{s}} + P\Gamma)$, where the matrices $I(\mathbf{s})$ and $B(\mathbf{s})$ depend only on the foil shape $\mathbf{s}$, and the matrix $P(\mathbf{s}, \Lambda)$ depends on the shape plus the locations of the vortices.

The remaining two items to summarize are 1) the motion of the point vortices and 2) how to add vortices. The motion of the vortices $\dot{\zeta}_k = p_k(\Xi, \Psi) = ((dW_k/dz) - (U + iV + i\Omega z_k) - (\partial F/\partial\zeta_c)\dot{\zeta}_c - (\partial F/\partial\alpha)\dot{\alpha})(1/F'(\zeta_k))$ and $W_k(z) = W(z) - i\gamma_k \log(z - z_k)$ is stated in [30] and is found using *Routh's rule* [18]. The point vortices are added to the system one by one at discrete points in time. The trailing edge of the foil (i.e., the stagnation point) is $(\alpha - \zeta_c)$ [30], while we choose the location of the new point vortex as $\zeta_n = 1.5(\alpha - \zeta_c)$. A review of different vortex locating methods (including simulations) can be found in [30]. The condition $dw(z_n)/d\zeta = 0$ must be satisfied to guarantee the stagnation point. The addition of the new vortex causes the effective fluid momenta to change, and thus, the body momentum must change as well. The discrete change in $\mathbf{U}$, which is denoted as $\Delta\mathbf{U}$, plus the strength of the new vortex γ_n, must satisfy $I\Delta\mathbf{U} + P\gamma_n = 0$, thus ensuring the conservation of momentum.

The calculation of $\mathbf{U}$ is split into: 1) intervals of time where (13) is used to find the body's translational and rotational velocities due to the body configuration and its shape velocities and 2) points in time where $dw(z_n)/d\zeta = 0$ and $I\Delta\mathbf{U} + P\gamma_n = 0$ are used to calculate the discrete change in the body velocities.

Thus, the complete dynamic system is given by

$$\dot{\Xi} = \begin{bmatrix} \dot{\zeta}_y \\ \dot{g} \\ \dot{\Lambda} \\ \dot{\Gamma} \end{bmatrix} = \begin{bmatrix} \Psi \\ l(\Xi, \Psi) \\ \Pi(\Xi, \Psi) \\ 0 \end{bmatrix} \tag{14}$$

$$\phi(x, y) = \eta[\Xi, \Psi](x, y) = \Re\{W(z)\} \tag{15}$$

where $\Pi(\Xi, \Psi) = [p_1(\Xi, \Psi)\ p_2(\Xi, \Psi)\ \ldots]^T$, and $l(\Xi, \Psi) = \Upsilon(\theta_f)\mathbf{U}(\Xi, \Psi)$. The initial condition for Λ is arbitrary, while the initial condition for Γ is zero. In this way, until a vortex is initialized, it has no effect on the system. To initialize, each ζ_k in Λ and γ_k in Γ are reset at time $k\Delta t$, and the reset is defined as $\zeta_k(k\Delta t) = 1.5(\alpha(k\Delta t) - \zeta_c(k\Delta t))$ and $\gamma_k(k\Delta t) = \nu_k$, where ν_k is the γ_n part of the solution to $dw(z_n)/d\zeta = 0$, and $I\Delta\mathbf{U} + P\gamma_n = 0$ at time $k\Delta t$, where $\zeta_n = \zeta_k$ and $\Delta\mathbf{U}$ are added to $\mathbf{U}(\Xi, \Psi)$ for use in $l(\Xi, \Psi)$.

B. Basic Gaits of the Joukowski Foil Fish

As shown in [30], the Joukowski foil fish, with the help of the shed vortices, will move forward and turn with the same input $\dot{\zeta}_y = a\omega\cos(\omega t)$, where the other shape parameters follow from the choice of ζ_y. The difference between the two gaits lies in the initial condition of ζ_y. The fish will move straight forward with the initial condition $\zeta_y|_{t=0} = 0$, while the fish will move around circles with the initial condition $\zeta_y|_{t=0} = \beta$ with $\beta \neq 0$ leading to

$$\zeta_y(t) = a\sin(\omega t) + \beta\,. \tag{16}$$

Figs. 9 and 10 show the fish moving forward and in a circle for various choices of parameters. Fig. 10 clearly shows the effect of the nondecaying vortices—the fish tail still moves with the same frequency, yet the period of resulting fish locomotion increases. Fig. 11 shows snapshots in time of the fish moving forward and the vortices that form.

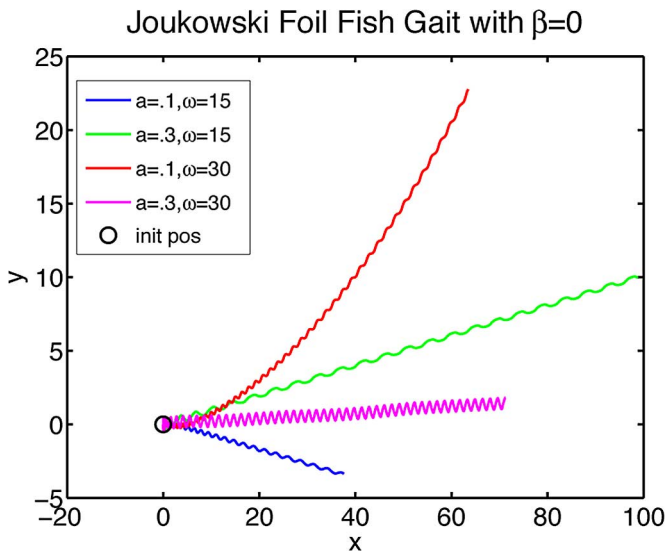

Fig. 9. Forward gait for Joukowski foil fish. $\beta = 0$.

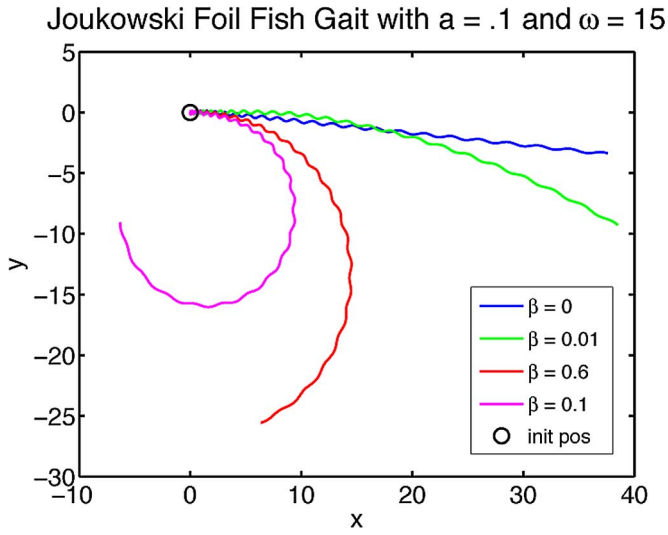

Fig. 10. Turning gait for Joukowski foil fish. $a = 0.1$, and $\omega = 15$.

C. Source Seeking for a Joukowski Foil Fish

As in Section IV-C, we notice that both the forward gait and turning gait have a sinusoidal term—similar to the probing term in the unicycle

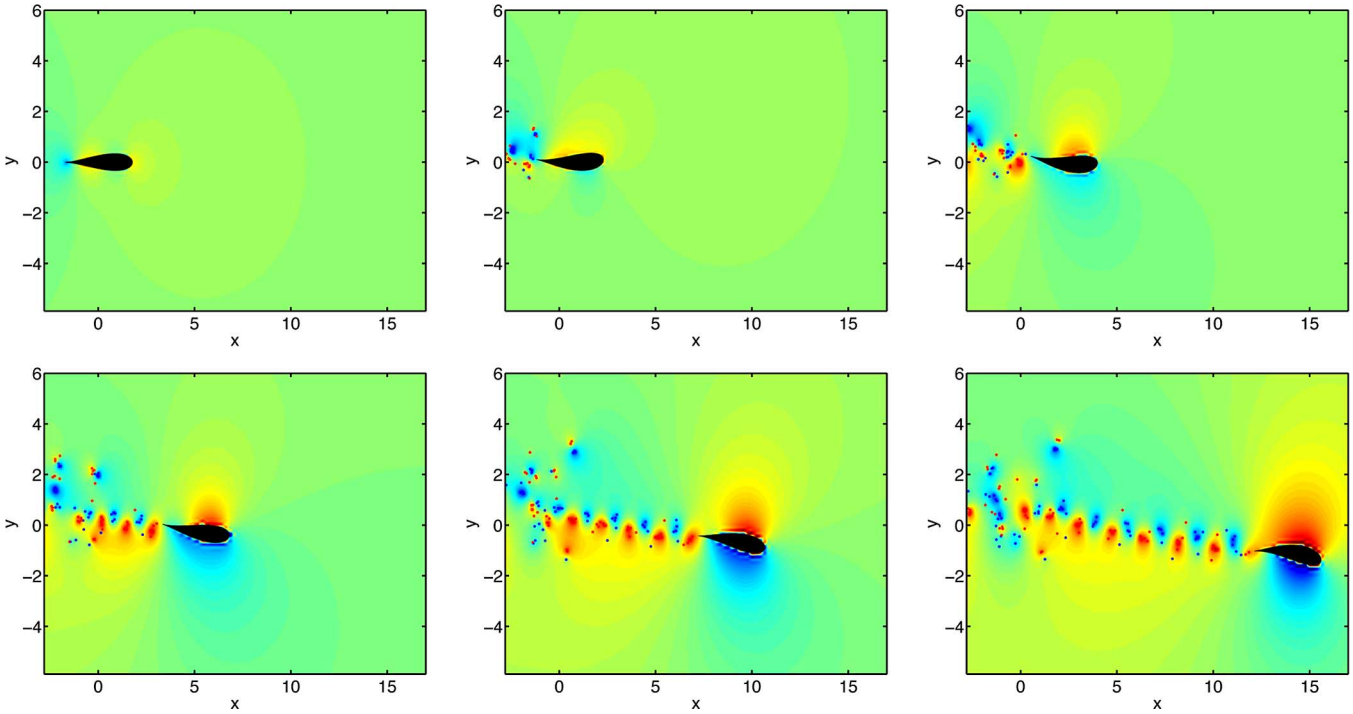

Fig. 11. Snapshots in time of a Joukowski foil fish moving forward. The background color field represents the stream/vorticity function ψ with red representing positive (clockwise) values and blue negative (counterclockwise). $a = 0.1$, and $\beta = 0$.

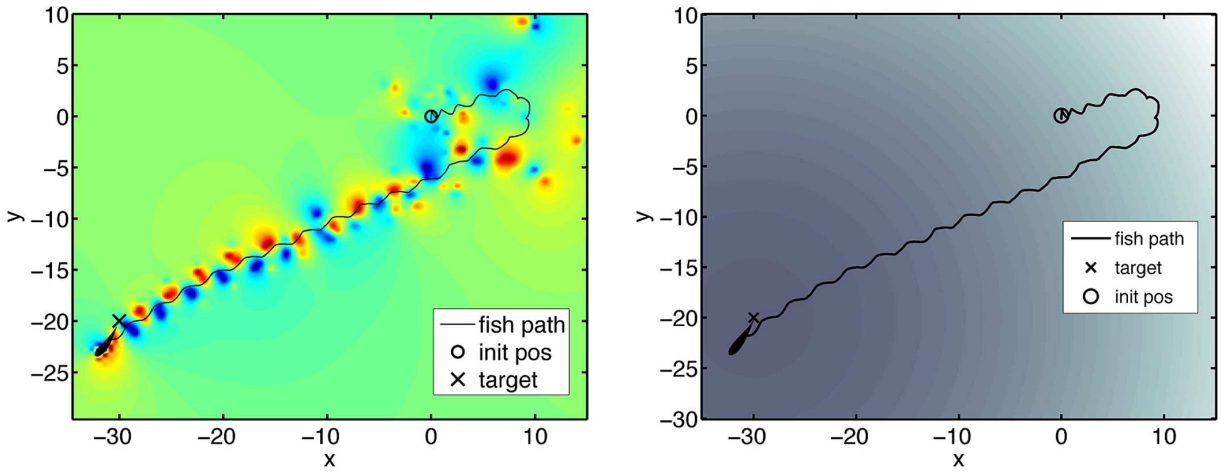

(a) (b)

Fig. 12. Source seeking for a Joukowski foil fish. (a) Background color field represents the stream/vorticity function ψ with red representing positive values and blue negative. (b) Background color field represents the "concentration" of the signal field J with the darker shade representing higher values than the lighter shade. $a = 0.3$, $c = 0.3$, $\omega = 20$, $h = 10$, $q_r = 10.2$, $r_c = 1$, and $\mu = 0.74$.

control law. We make β from (16) time-dependent and arrive at

$$\dot{\zeta}_y = a\omega\cos(\omega t) + c\xi\sin(\omega t) \tag{17}$$

$$\xi = H(s)[J], \qquad H(s) = \left(\frac{s}{s+h}\right)^2 \tag{18}$$

where our compensator $H(s)$ is a double washout filter. The function J that we wish to maximize is

$$J = -q_r\left((x^* - f_{sx})^2 + (y^* - f_{sy})^2\right) \tag{19}$$

$$f_s = (\mu + \frac{a^2}{\mu})\mathrm{e}^{j\theta_f} + f_x + if_y \tag{20}$$

where $f_s = (f_{sx}, f_{sy})$ is the location of the fish sensor, which is a forward point of the fish—its "nose." As mentioned previously, (x^*, y^*) is the goal location. Figs. 12 and 13 depict the fish going toward a target under the influence of (17).

While we constrain only the value of β in the control law for the three-link fish, we constrain both the value of β and its time derivative $\dot{\beta}$ for the Joukowski foil fish.

D. Path Following for a Joukowski Foil Fish

We modify the function J in the same way as we did in Section IV-D so that the Joukowski foil fish follows a predetermined path. Fig. 14

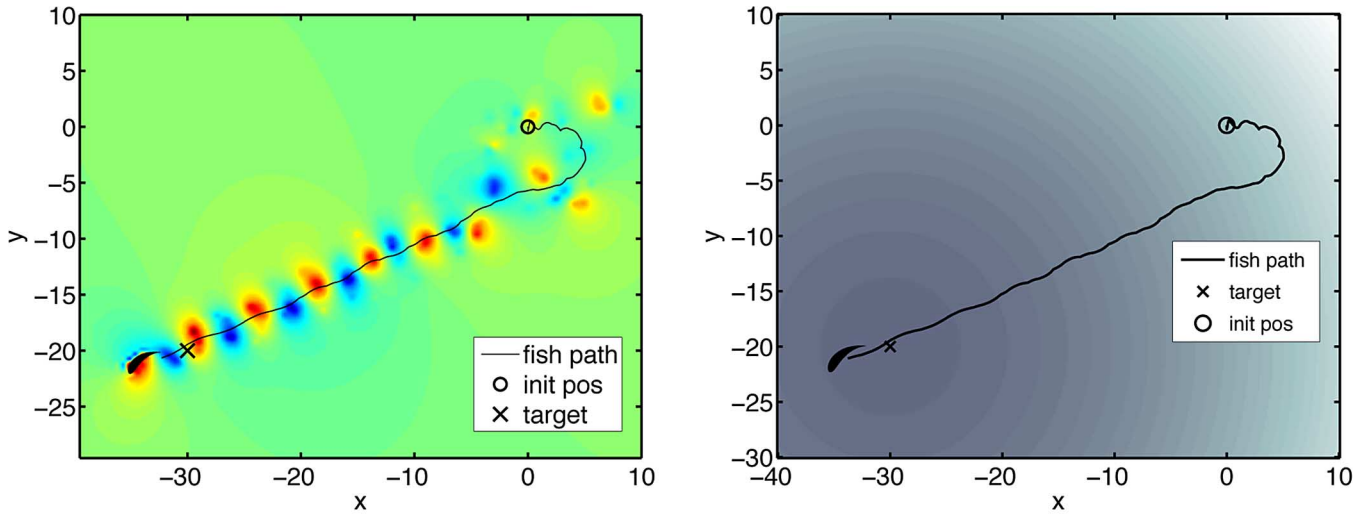

Fig. 13. Source seeking for a Joukowski foil fish. (a) Background color field represents the stream/vorticity function ψ with red representing positive values and blue negative. (b) Background color field represents the "concentration" of the signal field J with the darker shade representing higher values than the lighter shade. $a = 0.3$, $c = 0.3$, $\omega = 10$, $h = 10$, $q_r = 10.2$, $r_c = 1$, and $\mu = 0.74$.

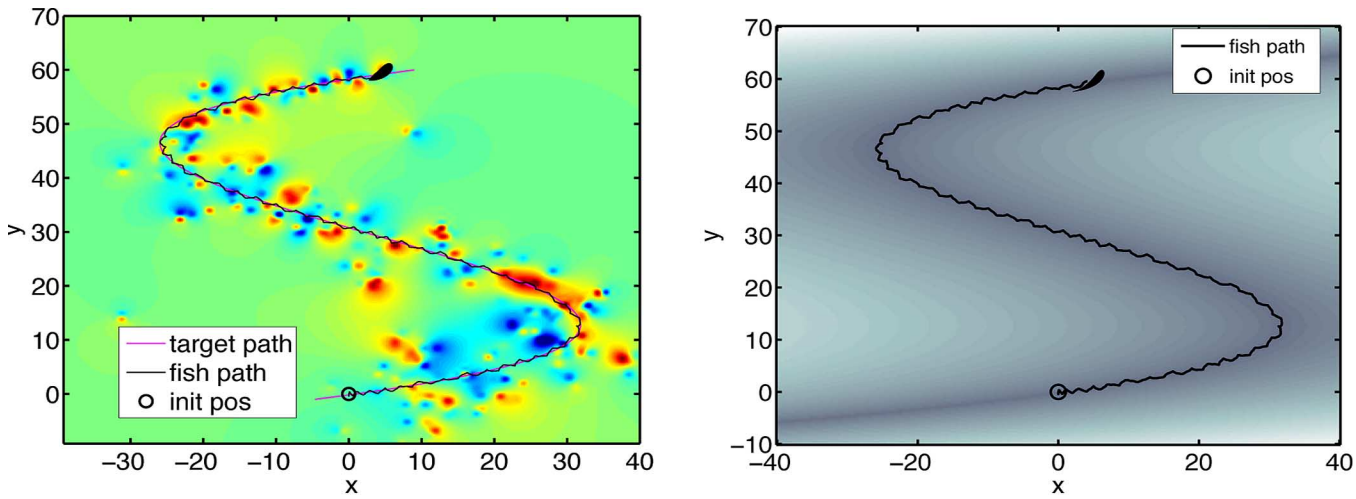

Fig. 14. Joukowski foil fish following a predetermined path. (a) Background color field represents the stream/vorticity function ψ with red representing positive values and blue negative. (b) Background color field represents the "concentration" of the signal field J with the darker shade representing higher values than the lighter shade. $a = 0.3$, $c = 10$, $\omega = 20$, $h = 20$, $r_c = 1$, and $\mu = 0.74$.

shows the path that the fish takes when following the path defined by

$$J = 300 \Big/ \sqrt{1 + \left| f_x - \left(\frac{3}{1000} f_y^3 - \frac{4}{15} f_y^2 + \frac{16}{3} f_y + 1 \right) \right|} \quad (21)$$

VI. Conclusion

We have shown that the sinusoid-based extremum-seeking method can steer underwater vehicles propelled by sinusoid-dominated body movement instead of motors. Readers might like to see detailed theoretical analyses such as those that we have completed for source seeking with nonholonomic vehicles in two [4] and three dimensions [5]. Such detailed results are beyond reach for the highly complex (and high dimensional) models in this paper; however, the theoretical intuition from [4] and [5] has guided the choices of the control laws (7)–(9), (17), and (18). Finally, in as much as the two models considered are realistic models of body fluid interaction taking place in locomotion of actual fish, the simple control laws (7)–(9), (17), and (18) seem as plausible feedback strategies that actual fish may be using to navigate gradient fields.

On an actual robotic three-link fish, each link would have a different mass. The first may be significantly heavier than the others, thereby affecting the gait. One would compensate the asymmetry by using different amplitudes of sinusoids. The asymmetry primarily affects the locomotion, rather than a source seeking. Source seeking would be used with different amplitudes of sunusoids, and even with different frequencies, as shown in [31].

APPENDIX

$$w_1(\zeta) = -\frac{r_c^2}{\zeta} + \zeta_c + \frac{\alpha^2}{(\zeta+\zeta_c)}, w_2(\zeta) = -i\left[\frac{r_c^2}{\zeta} + \zeta_c + \frac{\alpha^2}{(\zeta+\zeta_c)}\right]$$

$$w_3(\zeta) = \frac{-i}{2}\left[r_c^2 + 2\frac{\zeta_c r_c^2}{\zeta} + \delta^2 + 2\alpha^2\frac{(r_c^2/\zeta)+\zeta_c}{(\zeta+\zeta_c)} + \frac{\alpha^4(\zeta-\zeta_c)}{(\zeta+\zeta_c)(r_c^2-\delta^2)}\right] \tag{22}$$

$$\begin{aligned} w_{s1}(\zeta) = \Bigg[& -\frac{r_c^2}{\zeta} + \frac{\alpha^2 r_c^2}{\zeta\zeta_c^2} + \frac{\alpha^2}{(\zeta+\zeta_c)} \\ & - \frac{\alpha^4\zeta_c^2}{(\zeta+\zeta_c)(r_c^2-\delta^2)^2} - \frac{2\alpha^4 r_c^2\zeta_c}{(r_c^2-\delta^2)^3}\log\left(\frac{\zeta+\zeta_c}{r_c}\right) \\ & - \left(\frac{\alpha^2 r_c^2}{\zeta_c^3} - \frac{\alpha^2 r_c^2}{\zeta_c(r_c^2-\delta^2)^2}\right)\frac{\zeta}{(\zeta+\zeta_c)} \\ & - 2\alpha^2 r_c^2\left(\frac{1}{\zeta_c^3} + \frac{\zeta_c\alpha^2}{(r_c^2-\delta^2)^3}\right)\log\left(\frac{\zeta+\zeta_c}{\zeta}\right) \\ & + \frac{2\alpha^4 r_c^2(i\zeta_y)}{(r_c^2-\delta^2)^3}\log\left(\frac{\zeta}{r_c}\right)\Bigg] \end{aligned} \tag{23}$$

$$\begin{aligned} w_{s2}(\zeta) = (-i)\Bigg[& \frac{r_c^2}{\zeta} - \frac{\alpha^2 r_c^2}{\zeta\zeta_c^2} + \frac{\alpha^2}{(\zeta+\zeta_c)} \\ & - \frac{\alpha^4\zeta_c^2}{(\zeta+\zeta_c)(r_c^2-\delta^2)^2} - \frac{2\alpha^4 r_c^2\zeta_c}{(r_c^2-\delta^2)^3}\log\left(\frac{\zeta+\zeta_c}{r_c}\right) \\ & + \left(\frac{\alpha^2 r_c^2}{\zeta_c^3} - \frac{\alpha^2 r_c^2}{\zeta_c(r_c^2-\delta^2)^2}\right)\frac{\zeta}{(\zeta+\zeta_c)} \\ & + 2\alpha^2 r_c^2\left(\frac{1}{\zeta_c^3} + \frac{\zeta_c\alpha^2}{(r_c^2-\delta^2)^3}\right)\log\left(\frac{\zeta+\zeta_c}{\zeta}\right) \\ & + \frac{2\alpha^4 r_c^2\zeta_x}{(r_c^2-\delta^2)^3}\log\left(\frac{\zeta}{r_c}\right)\Bigg] \end{aligned} \tag{24}$$

$$\begin{aligned} w_{s3}(\zeta) = 2\alpha\Bigg[& -\frac{r_c^2}{\zeta\zeta_c} - \frac{\alpha^2\zeta_c}{(\zeta+\zeta_c)(r_c^2-\delta^2)} \\ & - \frac{\alpha^2 r_c^2}{(r_c^2-\delta^2)^2}\log\left(\frac{\zeta+\zeta_c}{r_c}\right) \\ & + \frac{r_c^2\left((r_c^2-\delta^2)^2 - \alpha^2\zeta_c^2\right)}{\zeta_c^2(r_c^2-\delta^2)^2}\log\left(\frac{\zeta+\zeta_c}{\zeta}\right)\Bigg] \end{aligned} \tag{25}$$

where $\delta = |\zeta_c|$.

REFERENCES

[1] K. Ariyur and M. Krstic, *Real-Time Optimization by Extremum-Seeking Control*. Hoboken, NJ: Wiley–Interscience, 2003.

[2] R. Becker, R. King, R. Petz, and W. Nitsche, "Adaptive closed-loop separation control on a high-lift configuration using extremum seeking," in *Proc. 3rd AIAA Flow Control Conf.*, vol. 45, no. 6, pp. 1382–1392, 2006.

[3] C. Centioli, F. Iannone, G. Mazza, M. Panella, L. Pangione, S. Podda, A. Tuccillo, V. Vitale, and L. Zaccarian, "Extremum seeking applied to the plasma control system of the Frascati Tokamak upgrade," in *Proc. 44th IEEE Conf. Decis. Control, Eur. Control Conf.*, 2005, pp. 8227–8232.

[4] J. Cochran and M. Krstic, "Nonholonomic source seeking with tuning of angular velocity," *IEEE Trans. Autom. Control*, vol. 54, no. 4, pp. 717–731, Apr. 2009.

[5] J. Cochran, A. Siranosian, N. Ghods, and M. Krstic, "3D source seeking for underactuated vehicles without position measurement," *IEEE Trans. Robot.*, vol. 25, no. 1, pp. 117–129, Feb. 2009.

[6] J. D. Eldridge, "Numerical simulation of the fluid dynamics of 2D rigid body motion with the vortex particle method," *J. Comput. Phys.*, vol. 221, pp. 626–648, 2007.

[7] E. Justh and P. Krishnaprasad, "Equilibria and steering laws for planar formations," *Syst. Control Lett.*, vol. 52, pp. 25–38, 2004.

[8] E. Kanso, J. E. Marsden, C. W. Rowley, and J. B. Melli-Huber, "Locomotion of articulated bodies in a perfect fluid," *J. Nonlinear Sci.*, vol. 15, pp. 255–289, 2005.

[9] S. D. Kelly and R. B. Hukkeri, "Mechanics, dynamics, and control of a single-input aquatic vehicle with variable coefficient of lift," *IEEE Trans. Robot.*, vol. 22, no. 6, pp. 1254–1264, Dec. 2006.

[10] R. King, R. Becker, G. Feuerbach, L. Henning, R. Petz, W. Nitsche, O. Lemke, and W. Neise, "Adaptive flow control using slope seeking," in *Proc. 14th IEEE Mediterr. Conf. Control Autom.*, 2006, pp. 1–6.

[11] D. Klein and K. Morgansen, "Controlled collective motion for trajectory tracking," in *Proc. Amer. Control Conf.*, 2006, pp. 5269–5275.

[12] M. Krstic and H. Wang, "Design and stability analysis of extremum seeking feedback for general nonlinear systems," *Automatica*, vol. 36, no. 2, pp. 595–601, 2000.

[13] Y. Li, A. Rotea, G. T.-C. Chiu, L. Mongeau, and I.-S. Paek, "Extremum seeking control of a tunable thermoacoustic cooler," *IEEE Trans. Control Syst. Technol.*, vol. 13, no. 4, pp. 527–536, Jul. 2005.

[14] R. J. Mason, "Fluid locomotion and trajectory planning for shape-changing robots," Ph.D. dissertation, Calif. Inst. Technol., Pasadena, 2002.

[15] E. Mbemmo, Z. Chen, S. Shatara, and X. Tan, "Modeling of biomimetic robotic fish propelled by an ionic polymer–metal composite actuator," in *Proc. IEEE Int. Conf. Robot. Autom.*, 2008, pp. 689–694.

[16] L. M. Milne-Thomson, *Theoretical Hydrodynamics*. New York: Dover, 1996.

[17] K. Morgansen, V. Duindam, R. Mason, J. Burdick, and R. Murray, "Nonlinear control methods for planar carangiform robot fish locomotion," in *Proc. IEEE Int. Conf. Robot. Autom.*, 2001, pp. 427–434.

[18] P. K. Newton, *The N-Vortex Problem*. New York: Springer-Verlag, 2001.

[19] P. Ogren, E. Fiorelli, and N. Leonard, "Cooperative control of mobile sensor networks: Adaptive gradient climbing in a distributed environment," *IEEE Trans. Autom. Control*, vol. 29, no. 8, pp. 1292–1302, Aug. 2004.

[20] Y. Ou, C. Xu, E. Schuster, T. Luce, J. R. Ferron, and M. Walker, "Extremum-seeking finite-time optimal control of plasma current profile at the DIII-D tokamak," in *Proc. Amer. Control Conf.*, 2007, pp. 4015–4020.

[21] K. Peterson and A. Stefanopoulou, "Extremum seeking control for soft landing of and electromechanical valve actuator," *Automatica*, vol. 29, pp. 1063–1069, 2004.

[22] B. Porat and A. Neohorai, "Localizing vapor-emitting sources by moving sensors," *IEEE Trans. Signal Process.*, vol. 44, no. 4, pp. 1018–1021, Apr. 1996.

[23] B. Protas, "Center manifold analysis of a point-vortex model of vortex shedding with control," *Physica D*, vol. 228, pp. 179–187, 2007.

[24] E. M. Purcell, "Life at low Reynolds number," *Amer. J. Phys.*, vol. 45, no. 1, pp. 3–11, Jan. 1977.

[25] B. N. Shashikanth, J. E. Marsden, J. W. Burdick, and S. D. Kelly, "The Hamiltonian structure of a 2-D rigid circular cylinder interacting dynamically with N point vortices," *Phys. Fluids*, vol. 14, pp. 1214–1227, 2002.

[26] A. M. O. Smith and J. L. Hess, "Calculation of potential flow about arbitrary bodies," *Prog. Aeronaut. Sci.*, vol. 8, pp. 1–139, 1966.

[27] Y. Tan, D. Nesic, and I. M. Y. Mareels, "On non-local stability properties of extremum seeking controllers," *Automatica*, vol. 42, pp. 889–903, 2006.

[28] M. Tanelli, A. Astolfi, and S. Savaresi, "Non-local extremum seeking control for active braking control systems," in *Proc. Conf. Control Appl.*, 2006, pp. 891–896.

[29] H. Wang and M. Krstic, "Extremum seeking for limit cycle minimization," *IEEE Trans. Autom. Control*, vol. 45, no. 12, pp. 2432–2436, Dec. 2000.

[30] H. Xiong, "Geometric mechanics, ideal hydrodynamics, and the locomotion of planar shape-changing aquatic vehicles," Ph.D. dissertation, Univ. Illinois at Urbana-Champaign, 2007.
[31] C. Zhang, D. Arnold, N. Ghods, A. Siranosian, and M. Krstic, "Source seeking with nonholonomic unicycle without position measurement and with tuning of forward velocity," *Syst. Control Lett.*, vol. 56, pp. 245–252, 2007.
[32] C. Zhang, A. Siranosian, and M. Krstic, "Extremum seeking for moderately unstable systems and for autonomous vehicle target tracking without position meas," *Automatica*, vol. 43, pp. 1832–1839, 2007.
[33] X. Zhang, D. Dawson, W. Dixon, and B. Xian, "Extremum seeking nonlinear controllers for a human exercise machine," in *Proc. IEEE Conf. Decis. Control*, 2004, pp. 3950–3955.

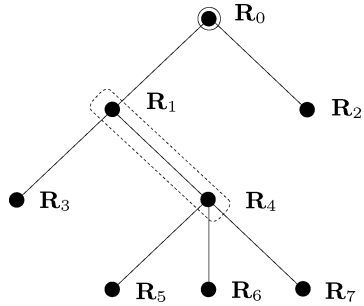

Fig. 1. Structure of a simple hierarchical formation. The *main leader* $\mathbf{R}_0$ guides the formation. One of the seven *leader–follower units* is highlighted: $\mathbf{R}_1$ is the *relative leader* of $\mathbf{R}_4$. Robots $\mathbf{R}_5$, $\mathbf{R}_6$, and $\mathbf{R}_7$ act only as followers in the formation.

Stabilization of a Hierarchical Formation of Unicycle Robots with Velocity and Curvature Constraints

Luca Consolini, *Member, IEEE*,
Fabio Morbidi, *Student Member, IEEE*,
Domenico Prattichizzo, *Member, IEEE*, and Mario Tosques

***Abstract*—The paper proposes a new geometric approach to the stabilization of a hierarchical formation of unicycle robots. Hierarchical formations consist of elementary leader–follower units disposed on a rooted tree: each follower sees its relative leader as a fixed point in its own reference frame. Robots' linear velocity and trajectory curvature are forced to satisfy some given bounds. The major contribution of the paper is to study the effect of these bounds on the admissible trajectories of the main leader. In particular, we provide recursive formulas for the maximum velocity and curvature allowed for the main leader, so that the robots can achieve the desired formation while respecting their input constraints. An original formation control law is proposed and the asymptotic stabilization is proved. Simulation experiments illustrate the theory and show the effectiveness of the proposed designs.**

***Index Terms*—Formation control, mobile robots, motion control, multiagent systems, nonlinear systems.**

I. Introduction

Recent years have witnessed a growing interest in robotics, in motion coordination and cooperative control of multiagent systems [1]–[3]. In this respect, several new problems, such as, e.g., *consensus* [4], [5], *rendezvous* [6], [7], *coverage* [8], *connectivity maintenance* [9], [10], and *formation control*, have been formulated and solved using tools coming from computer science and control theory. Among them, for its wide range of applicability, the formation control problem received a special attention and stimulated a great deal of research [11]–[15]. By formation control, we simply mean the problem of controlling the relative position and orientation of the robots in a group while allowing the group to move as a whole. Typical working scenarios of robot formations are terrain and utilities inspection, disaster monitoring, environmental surveillance, search and rescue, structures moving and assembling, and planetary exploration. Research on formation control dealt with ground vehicles [16], [17], autonomous underwater vehicles (AUVs) [18], [19], unmanned aerial vehicles (UAVs) [20], [21], and microsatellites [22], [23].

One of the main approaches to formation control is *leader-following* [24]–[26]. A robot of the formation, designed as the leader, moves along a predefined trajectory, while the other robots, the followers, are to maintain a desired distance and orientation to the leader. Leader–follower architectures are known to have poor disturbance rejection properties. In addition, the overreliance on a single agent to achieve the goal may be undesirable, especially in adverse conditions. Nevertheless, the leader–follower approach is particularly appreciated for its simplicity and scalability.

This paper extends our previous work [27] on the stabilization of a leader–follower pair of robots, to *hierarchical formations* of unicycles with input constraints. Hierarchical formations are characterized by elementary *leader–follower units,* whose interconnection is described by a rooted tree graph (see Fig. 1). The *main leader* $\mathbf{R}_0$ drives the formation, while all the other robots $\mathbf{R}_i$ act both as followers and leaders (with the exception of the leaves of the tree, which are only followers).

The original contribution of this paper with respect to the existing literature is twofold.

1) Each follower in the formation has to maintain a desired distance and orientation to its *relative leader* with respect to *its own local* reference frame.

2) The velocity and the curvature admissible for each follower in the formation are assumed to be *bounded*. The maximum velocity and curvature that are allowed for the main leader are determined through recursive formulas and a stabilizing controller is designed for each robot, so that the desired formation is asymptotically achieved and the input constraints are respected.

A peculiar feature of the proposed control strategy is that at steady state the whole formation is not rigid but changes its shape according to the motion of the main leader. Each follower's position is not fixed in the reference frame of its relative leader, but it varies in time in a suitable circle arc fixed in the relative leader's frame.

The rest of the paper is organized as follows. In Section II, some basic definitions are provided and the problem studied in the paper is formulated. In Sections III and IV, an original solution to the stabilization

Manuscript received June 4, 2009. First published September 11, 2009; current version published October 9, 2009. This paper was recommended for publication by Associate Editor W. Chung and Editor K. Lynch upon evaluation of the reviewers' comments.

L. Consolini is with the Department of Information Engineering, University of Parma, Parma 43100, Italy (e-mail: lucac@ce.unipr.it).

F. Morbidi and D. Prattichizzo are with the Department of Information Engineering, University of Siena, Siena 53100, Italy (e-mail: morbidi@dii.unisi.it; prattichizzo@dii.unisi.it).

M. Tosques is with the Department of Civil Engineering, University of Parma, Parma 43100, Italy (e-mail: mario.tosques@unipr.it).

Color versions of one or more of the figures in this paper are available online at http://ieeexplore.ieee.org.

Digital Object Identifier 10.1109/TRO.2009.2026505